Sodium Sensing in Neurons with a Dendrimer-Based Nanoprobe

Christophe M. Lamy,[†,*] Olivier Sallin,[†,‡] Céline Loussert,[§] and Jean-Yves Chatton[†,‡]

[†]Department of Cell Biology and Morphology, [‡]Cellular Imaging Facility, and [§]Electron Microscopy Facility, University of Lausanne, Rue du Bugnon 9, CH-1005 Lausanne, Switzerland

ABSTRACT

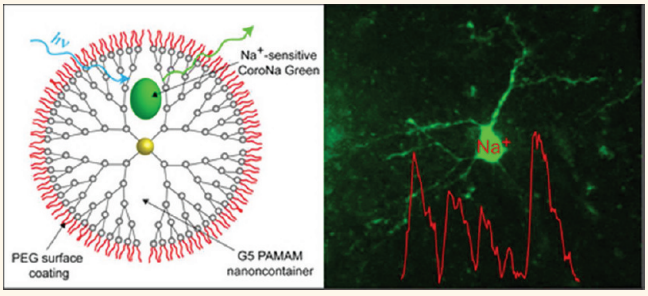

Ion imaging is a powerful methodology to assess fundamental biological processes in live cells. The limited efficiency of some ion-sensing probes and their fast leakage from cells are important restrictions to this approach. In this study, we present a novel strategy based on the use of dendrimer nanoparticles to obtain better intracellular retention of fluorescent probes and perform prolonged fluorescence imaging of intracellular ion dynamics. A new sodium-sensitive nanoprobe was generated by encapsulating a sodium dye in a PAMAM dendrimer nanocontainer. This nanoprobe is very stable and has high sodium sensitivity and selectivity. When loaded in neurons in live brain tissue, it homogenously fills the entire cell volume, including small processes, and stays for long durations, with no detectable alterations of cell functional properties. We demonstrate the suitability of this new sodium nanosensor for monitoring physiological sodium responses such as those occurring during neuronal activity.

KEYWORDS: PAMAM dendrimer · nanoprobe · fluorescence imaging · neuron · sodium

Fluorescence imaging is widely used in biomedical sciences for a large spectrum of applications ranging from the morphological analysis of anatomical structures to time-resolved measurements of intracellular molecular events.[1,2] It enables noninvasive probing of biological processes with high spatial resolution in *ex vivo* tissue preparations as well as in whole organisms.[3,4] A powerful application of this technique is the ability to monitor in real-time the complex intracellular fluxes of ions and metabolites that underlie many essential physiological functions.[5,6] Most studies so far focused mainly on imaging Ca^{2+} as a ubiquitous secondary signal giving large amplitude, easily detectable responses. Other key cellular ions such as Na^+, K^+, and Cl^- that give more elusive responses proved more difficult to measure.[7−10] As a result, detailed knowledge of their temporal and spatial dynamics is still largely missing. Sodium imaging, in particular, is an attractive way of assessing many fundamental cellular processes, from the transport of small molecules through epithelial barriers to the integration of complex signals in the brain, that depend on the transmembrane Na^+ gradient. Unlike Ca^{2+} signals, Na^+ changes are a more direct reflection of primary cellular mechanisms, and their measurement is not hampered by buffering of responses by cytosolic proteins or by the indicator itself.[4,11] However, the poor characteristics of available Na^+ probes have rendered Na^+ imaging an uneasy task.[8,12]

Most existing ion-sensitive sensors are small fluorescent dyes. Sodium imaging has relied so far mainly on fluorescent dye sodium-binding benzofuran isophthalate (SBFI[7]). This compound requires UV excitation which is suboptimal for imaging deep in tissue due to the strong scattering of UV photons and results in phototoxic damage.[13] Attempts to generate better Na^+ dyes produced several candidates. Sodium Green was one noticeable alternative,[14] but it produced inaccurate Na^+ measurements due to interactions with cell proteins.[12] CoroNa Green (CG) was another promising attempt, but it suffered from a fast efflux from cells after loading.[8,15]

More recently, fluorescent nanoprobes were developed and used for fluorescence microscopy. These include quantum dots, silicon and carbon nanoparticles, nanophosphors, and gold−silver nanocages.[16−22] Nanoparticles usually provide bright and stable signal over time. They can remain in cells for days or longer.[20] However, they are not intrinsically sensitive to ion concentrations and need further engineering

* Address correspondence to christophe.lamy@unil.ch.

Received for review October 5, 2011 and accepted January 30, 2012.

Published online January 30, 2012
10.1021/nn203822t

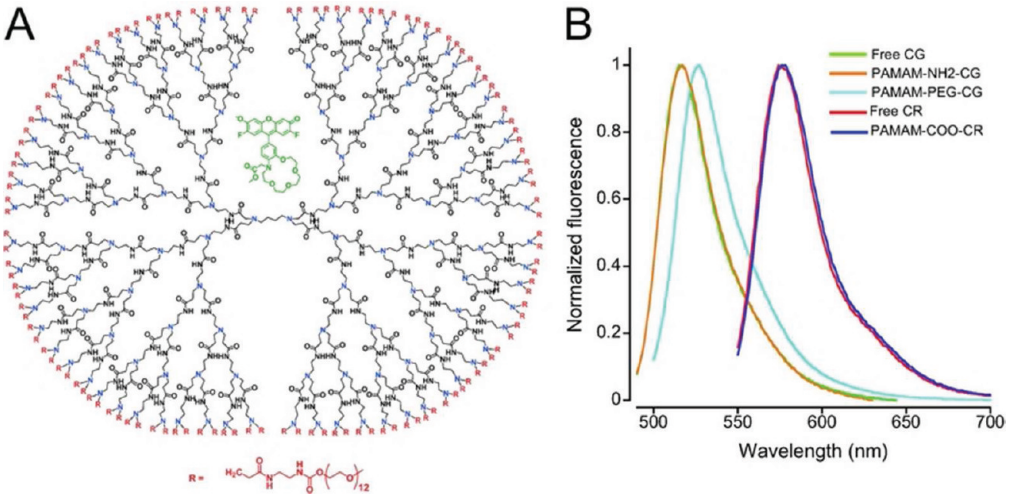

Figure 1. Dendrimer-based sodium-sensitive fluorescent nanoprobes. (A) Sketch representing the idealized principle of a nanoprobe composed of a G5 PAMAM-PEG dendrimer with Na^+ dye CoroNa Green encapsulated in one of the cavities (green). Tertiary amines (in blue) are thought to play an important role in the dye encapsulation. Estimated size = 6.5 nm, estimated molecular mass = 104 kDa. (B) Fluorescence emission spectra of CoroNa Green (λ_{ex} = 495 nm), CoroNa Red (λ_{ex} = 556 nm), and derived PAMAM-based nanoprobes.

to obtain fluorescent ion sensors. Quantum-dot-based K^+, Cl^-, and pH-sensitive sensors have been reported.[23−26] Similarly, a very elegant approach was used to make a Na^+ nanosensor by embedding a quantum dot in an ion-selective polymer containing a pH indicator. This sensor showed good Na^+ sensitivity and selectivity *in vitro*, but its Na^+ responsiveness was not demonstrated in a live cell yet.[27] Na^+ nanosensors made of a polymer/ionophore/chromoionophore combination without quantum dots were also devised and proved to detect efficiently Na^+ transients in cultured cells.[15,28−30] An important disadvantage of these nanoprobes is their large size, typically over 100 nm in diameter,[28,30] which is likely to limit their diffusion in smaller cell compartments, such as axons and dendrites of neurons, where most of the cell's biological activity is often concentrated. In addition, their loading often requires invasive procedures like picoinjection or biolistic delivery that can damage living cells.[15]

Making good fluorescent probes for live imaging is quite challenging. Requirements for an ideal ion-sensitive molecule are excitation with visible or near-infrared light, a safe delivery to cells, targeting to the appropriate subcellular compartment, absence of cell leakage or photobleaching, absence of interaction with cellular physiology, absence of cytotoxicity, high selectivity to the ion species studied, affinity for the target in the physiological range, high brightness, and large fluorescence changes during physiological responses (for review, see ref 31). An alternative to the complex design of new fluorescent dyes is to use existing ones and find ways to improve their usage. CG, for instance, was loaded in neurons with a patch-clamp pipet to compensate its fast leakage. However, this led to inaccurate Na^+ measurements.[8] Another strategy to avoid rapid efflux of a dye from cells is to tether it to a large molecule like a dextran. This proved successful for calcium dyes but is complicated by the need for a covalent attachment.[32]

We thought to use dendrimers to improve the cellular retention of existing dyes without the need of covalent chemistry. Dendrimers are branched polymers with well-defined sizes and geometry. After several layers of branching, they make spheres that contain solvent-filled cavities. These structural features endow them with the ability to encapsulate small guest molecules and act as nanocontainers. Dendrimer nanocontainers have been extensively used for drug and gene delivery applications.[33−35] Efficient encapsulation of fluorescent dyes by dendrimers has also been reported.[36,37] However, this property has not been used in molecular imaging yet. In this study, we tested whether a Na^+ dye such as CG could be encapsulated in a dendrimer in order to prolong its intracellular half-life while maintaining its Na^+ response characteristics. We also assessed whether a Na^+ nanoprobe built on this principle could be used to probe cell functions in thick tissue preparations without disturbing baseline physiological parameters.

RESULTS AND DISCUSSION

We generated Na^+ sensing nanoprobes using Tomalia-type poly(amidoamine) (PAMAM) dendrimers[34,35,38] doped with Na^+-sensitive dyes CG and CoroNa Red (CR). We choose generation 4.5 or 5 (G4.5-G5) dendrimers to take advantage of the nanocontainer property of the nanoparticle and enable encapsulation of the guest fluorescent dye while maintaining a good communication of the dendritic cavity with the external medium. PAMAM dendrimers smaller than G3 do not allow encapsulation, whereas for generations

higher than G6, surface congestion impairs access to the dendrimer interior.[35] Three Na^+ nanosensor designs were tested. CG was combined with G5 dendrimers carrying either an amidoamine (PAMAM-NH_2-CG) or a poly(ethyleneglycol) (PAMAM-PEG-CG, Figure 1A) surface. CR, a positively charged molecule, was used in conjunction with a G4.5 dendrimer functionalized with a sodium carboxylate surface (PAMAM-COONa-CR). We used a limiting dye/dendrimer ratio of 1.2 in order to avoid having multiple dye molecules associated with the same dendrimer particle that could result in self-quenching of the fluorescence.[39,40] To demonstrate the stability of these complexes, we performed exhaustive ultrafiltration with a 3 kDa cutoff membrane allowing the separation of complexes (~30 000–100 000 Da) and host (~600 Da). After four rounds of washing with HEPES buffer, the complexes were retained in the filtration cell while the unbound dye molecules were collected in the flow-through and quantified by UV–vis spectrometry. The bound fraction of the dye was found to be 68.3% for PAMAM-PEG-CG, 91.3% for PAMAM-NH_2-CG, and 100% for PAMAM-COONa-CR. The final dye/dendrimer stoichiometry was therefore 0.82 for PAMAM-PEG-CG, 1.10 for PAMAM-NH_2-CG, and 1.20 for PAMAM-COO-CR.

The different dye binding capacity of PAMAM-PEG-CG and PAMAM-NH_2-CG indicates a different mode of complexation of the dye with host dendrimers. We performed further measurements to gain insight on this interaction. Organic acids were shown to be preferentially retained in the inner cavities of water-soluble dendrimer cavities as a result of electrostatic interactions with internal tertiary amines.[41–44] Tertiary amines in the PAMAM dendrimer core are known to be more acid than the primary amine groups in the periphery (pK_a = 6.65 and 9.20, respectively[43]). At pH 7.4, most of the surface primary amines are positively charged while 85% of interior amine groups are uncharged. We did an acid–base titration of free CG and obtained a pK_a of 5.04, meaning that in our conditions almost all CG molecules are negatively charged. In PAMAM-NH_2-CG, CG is thus likely to mainly interact with the surface amines. In PAMAM-PEG-CG, the outer shell of PEG is electroneutral and does not offer strong enough interactions to stabilize the dye on the nanoprobe. To check if the affinity of PAMAM-PEG for CG is related to acid–base interactions, we prepared a batch of PAMAM-PEG-CG nanoprobe at pH 6. In this condition, the binding capacity of the dendrimer should become higher as the number of protonated internal amines increase while CG remains largely deprotonated. After ultrafiltration, the dye-bound fraction increased to 78.3%, demonstrating that electrostatic interactions are important for the retention of CG. We then used fluorescence anisotropy, reflecting the rotational freedom of fluorescent molecules, as a way to probe the host–guest interaction.[37] Steady-state fluorescence anisotropy values were found to be significantly higher for PAMAM-PEG-CG ($r = 0.208 \pm 0.002$, $p = 0.0001$) and PAMAM-NH_2-CG ($r = 0.145 \pm 0.004$, $p = 0.0004$) than for free CG ($r = 0.116 \pm 0.003$), confirming that CG is closely associated with the nanoparticles. These measurements indicated that anisotropy was significantly higher for PAMAM-PEG-CG than for PAMAM-NH_2-CG ($p = 0.0001$). This result is compatible with CG being entrapped in the dendrimer cavity of PAMAM-PEG,[45] resulting in a greater reduction in rotational freedom than in the case of PAMAM-NH_2-CG where the dye is thought to be primarily associated with the shell terminal amines.

To assess whether the association with the dendrimer would alter the dyes' spectral properties, we acquired the fluorescence emission spectra of the three nanoprobes and of the corresponding free dyes *in vitro* in a buffer having a similar ionic strength and pH as the intracellular environment. The emission spectra of PAMAM-NH_2-CG and PAMAM-COONa-CR were identical to the emission spectra of free CG and CR, respectively (Figure 1B). In contrast, the emission spectrum of PAMAM-PEG-CG showed a bathochromic shift in the wavelength of the emission maximum of 12 nm as compared to free CG (Figure 1B). This shift is an indication of a complex formation between the dendrimer host and the dye guest as was previously reported for other anionic dyes such as Rose Bengal and tetrachlorofluorescein.[41] To confirm this complexation, we measured the absorption spectra of free CG and PAMAM-PEG-CG. Similarly to fluorescence emission, we observed a 12 nm bathochromic shift in the wavelength of the absorption maximum with the nanoprobe (Figure S1 in Supporting Information). These spectra were measured on dendrimer–dye complexes after the removal of unbound dye by ultrafiltration. Similar full width at half-maximum values show that the spectra of the complexes are not altered by the presence of contaminating free dye. In addition, spectra of the PAMAM-PEG-CG nanoprobe generated more than a month later were unchanged, suggesting that there is no significant dye leaching from the complexes. To confirm the probe's stability *in vitro*, we measured the amount of dye separating from the dendrimer over time. The fraction of unbound CG measured by spectrophotometry increased by 1.6% over a storage period of 1 month.

We then tested the performance of our nanoprobes for measuring Na^+. We recorded the fluorescence emission spectra of dyes and of dye–dendrimer complexes in buffers containing graded Na^+ concentrations (Figure 2A,B). Fluorescence intensity of all nanoprobes increased with [Na^+]. Peak amplitudes of spectra were plotted against [Na^+]. Except for PAMAM-COONa-CR, the relationship between [Na^+] and normalized changes in fluorescence showed remarkable linearity in the physiologically relevant 0–50 mM

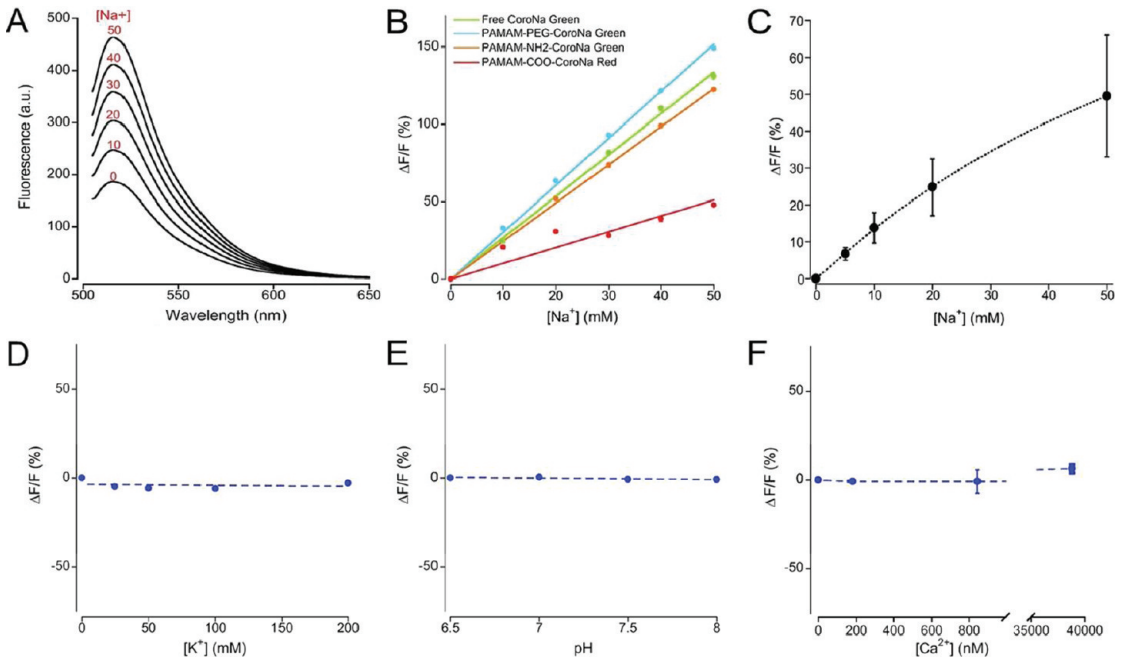

Figure 2. Sodium dependency and selectivity of nanoprobes. (A) Emission spectra of PAMAM-PEG-CG measured at different Na^+ concentrations *in vitro* (λ_{ex} = 495 nm). (B) *In vitro* Na^+ calibration curves for CoroNa Green, PAMAM-PEG-CG, PAMAM-PEG-NH_2-CG, and PAMAM-COONa-CR show the relative performance of these sensors to detect [Na^+] changes. Colored lines represent linear fits to calibration values (R^2 = 0.999, 0999, 0.998, and 0.867, respectively, n = 9). Data are percent fluorescence changes from 0 mM [Na^+] ± SEM. (C) *In situ* Na^+ calibration curve for PAMAM-PEG-CG performed in HEK-293 cells indicates a lower sensitivity of the probe for Na^+ when loaded in cells than *in vitro*. Fit of data points with the Hill equation (dotted line, R^2 = 0.999, n = 5) gives estimates of apparent K_d = 81.2 mM and $(\Delta F/F_o)_{max}$ = 131.2%. Data are percent fluorescence changes from 0 mM [Na^+] ± SEM. (D–F) *In vitro* sensitivities of PAMAM-PEG-CG to variations in [K^+], pH, and [Ca^{2+}] were tested measuring changes in probe's fluorescence when varying the concentration of respective parameters in the presence of 20 mM Na^+. Data are percent fluorescence changes from 0 mM [K^+], pH 6.5, and 0 mM [Ca^{2+}], respectively, ± SEM (n = 9).

Na^+ range (Figure 2B). Na^+ sensitivity was higher for PAMAM-PEG-CG than for free CG. This interesting property might be due to restricted movements inside the cavity, resulting in reduced nonradiative relaxation and an increased fluorescence lifetime.[45,46] Differences in the local nanoenvironment polarity as compared to the bulk solution and reduction of concentration quenching due to a larger distance between fluorescent molecules could also contribute to this increased fluorescent response.[46,47] PAMAM-NH_2-CG was less sensitive to Na^+ than both PAMAM-PEG-CG and free CG. We attribute this observation to the repulsion of Na^+ by the positively charged surface of PAMAM-NH_2.[48] PAMAM-COONa-CR had the poorest Na^+ response curve. This could be explained by the quenching of CR fluorescence and the local buffering of Na^+ by PAMAM-COONa surface carboxylate groups.[49,50] Since PAMAM-PEG-CG gave the best responses to Na^+, we decided to focus on this nanoprobe for the remainder of the study.

Responsiveness of fluorescent probes once they are loaded in cells can differ substantially from the *in vitro* situation. We thus performed an *in situ* calibration of PAMAM-PEG-CG in HEK-293 cells. Fluorescence change with [Na^+] was smaller, and the probe saturated for lower [Na^+] *in situ* than *in vitro* (Figure 2C). The calibration curve could be fitted by the Hill equation (R^2 = 0.999, n = 5, Figure 2C), which allowed us to estimate the apparent K_d at 81.2 mM and the maximum change in relative fluorescence at 131.2%. These values are close to supposed values for free CG in neurons.[8]

A concern with measuring cytosolic Na^+ is the possible interference of simultaneously varying concentrations of other intracellular ions. The main cytosolic monovalent cation is K^+. We tested the sensitivity of PAMAM-PEG-CG to K^+ and found no significant effect over a large concentration range (R^2 = −0.298, p = 0.794, Figure 2D). Intracellular pH can also vary during cellular activation and affect the efficiency of fluorescent probes. PAMAM-PEG-CG was not significantly influenced by pH in a physiological range (R^2 = 0.445, p = 0.206, Figure 2E). Ca^{2+} transients are ubiquitous intracellular signals. In neurons, they accompany firing of action potential and synaptic transmission. The nanoprobe did not respond to Ca^{2+} over a wide concentration range (R^2 = −0.259, p = 0.588, Figure 2F).

The properties of the Na^+ nanosensor were further studied in the intracellular environment. PAMAM-PEG-CG was loaded in a glass pipet and delivered to live neurons in acute neocortical brain slices by single-cell electroporation (Figure 3A). This method was shown to be a safe way to deliver charged macromolecules to neurons.[51] We used this approach instead of whole-cell patch-clamp to avoid altering Na^+ responses by

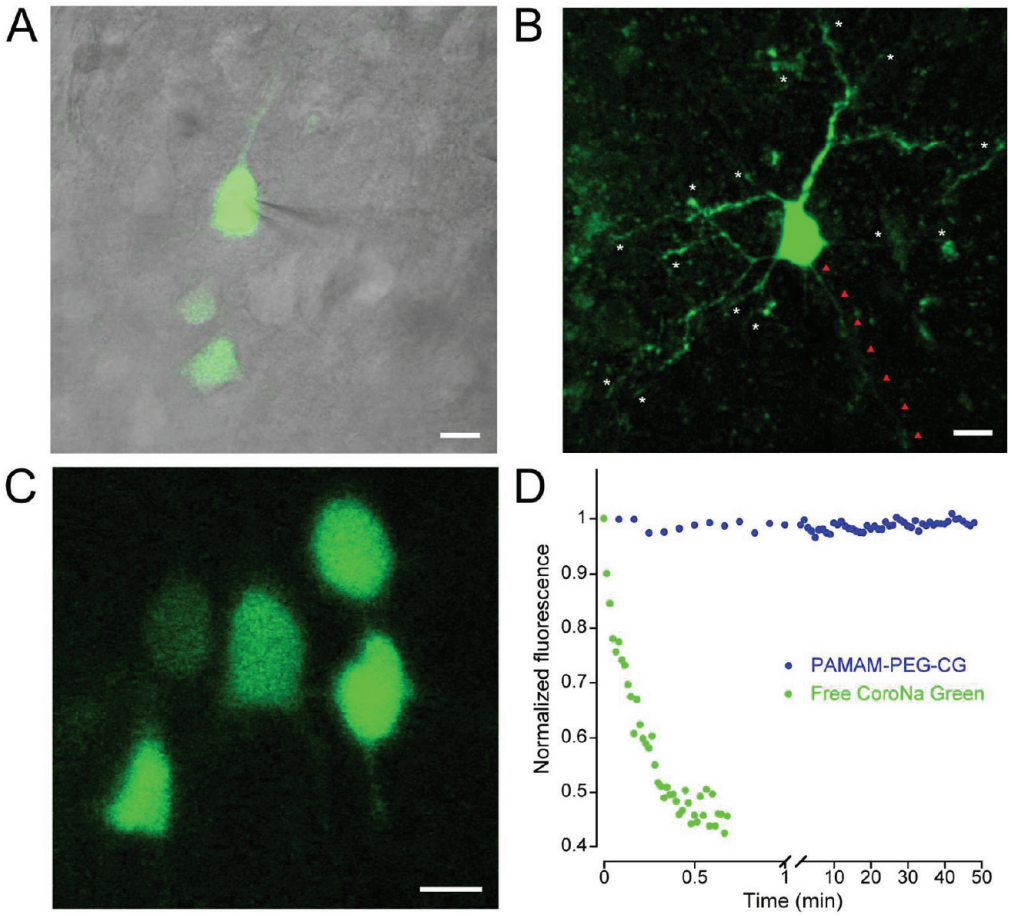

Figure 3. Loading of sodium-sensing nanoprobe in neurons in brain slices. (A) Fluorescent image of cortical pyramidal neurons loaded with PAMAM-PEG-CG superimposed to a differential interference contrast (DIC) image of the brain slice. The pipet used for loading the nanoprobe by single-cell electroporation appears on the right side of the larger neuron. (B) Maximum intensity projection of a 3D confocal image stack acquired through a neuron loaded with PAMAM-PEG-CG shows the homogeneous diffusion of the probe far away in dendrites (white arrowheads) and the axon (red arrowheads). (C) Single-cell electroporation enabled multicell loading of neighboring neurons in brain slices. On this nonconfocal image taken at a single focal plane, neurons located at different depth in the slice appear with different fluorescence intensities. (D) Representative time courses of baseline fluorescence monitored continuously in neurons loaded either with free CoroNa Green or with PAMAM-PEG-CG show that the dendrimer shell enables prolonged intracellular retention of the dye. Scale bars, 10 μm.

dilution with the pipet solution.[8,52] With this technique, we were able to specifically target the nanoprobe to selected cells (Figure 3B). We could also sequentially fill multiple cells if needed (Figure 3C). The nanoprobe diffused rapidly through the entire cell volume including to dendrites and the axon (Figure 3B), indicating that the size of the nanoparticle is not an obstacle for imaging remote small cellular compartments. The size of PAMAM-PEG-CG nanoparticles was measured by transmission electron microscopy (TEM) using uranyl acetate as a contrast agent (Figure 4). The average particle diameter measured from TEM images was 6.57 ± 0.04 nm ($n = 1785$ particles). This size is in agreement with the diameter of 6.5 nm estimated from average C−C and C−N bonds lengths and with the sizes measured with other techniques for G5 dendrimers.[53−56] PAMAM-PEG-CG nanoparticles are thus much smaller than previously published Na^+ nanosensors.[28−30] Those gave less homogeneous patterns of fluorescence than the one we observed, probably due to the larger volume and more inhomogeneous shape of the probes, leading to some degree of intracellular clustering.

The main reason for devising a CG-doped nanoparticle instead of using CG alone was the extremely fast leakage of this dye from living cells. PAMAM-PEG-CG intracellular fluorescence baseline in slice neurons was stable over the duration of experiments (typically more than 1 h), in sharp contrast with the fast decay of CG fluorescence (Figure 3D). The slow residual decay in fluorescence is likely due to CG photobleaching as indicated by its faster rate when laser illumination was increased. Previously described nanoprobes suffered from component leaching.[15,28,30] If this were the case with PAMAM-PEG-CG, unbound CG would exit from cells very fast after the loading of the nanoprobe. This would lead to a rapid initial drop in fluorescence, which we did not observe. Furthermore, the fact that

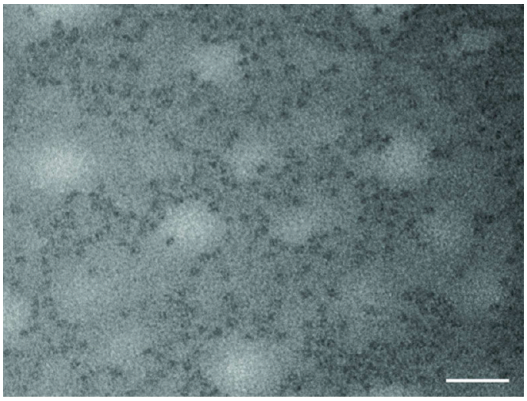

Figure 4. Transmission electron microscopy image of PAMAM-PEG-CG nanoprobes positively stained with 4% uranyl acetate shows a monodisperse population of particles with little aggregation. Nanoparticles appear as dark circular elements due to the uptake of the contrast agent. Their average size was measured at 6.57 ± 0.04 nm. Scale bar, 50 nm.

the same batch of nanoprobe could be used over weeks without any significant leakage indicates that there is no dye leaching from the probe, confirming the stability we observed *in vitro*.

A frequent concern with nanoparticles is their cytotoxicity.[35] We addressed this issue in a separate set of experiments by recording the functional properties of neurons using whole-cell electrophysiology. Passive membrane properties, cell excitability, and action potential characteristics were identical in neurons filled with PAMAM-PEG-CG and control neurons (Table 1). These data indicate that our dendrimer-based nanosensor does not alter essential cell functions. It is noteworthy that Na^+-dependent electrical responses like action potentials were unaffected, ruling out any interference of the nanosensor with the measured parameter. Since neurons are extremely sensitive to any modification of their internal environment, we can safely extrapolate that PAMAM-PEG-CG will be harmless to most other cell types. Innocuousness of this nanoprobe is attributable to the external coating with PEG, a functional group previously shown to increase biocompatibility.[57,58] In our experience, dendrimers with charged surfaces, such as PAMAM-NH_2 and PAMAM-COONa, induced microscopic alterations indicative of cell suffering. We conclude from these characteristics that our Na^+ nanoprobe can be used safely for prolonged measurements of Na^+ responses in live cells.

Measurements of physiological Na^+ responses were performed in brain slices in layer 2/3 neocortical neurons loaded with PAMAM-PEG-CG as described earlier. We first induced neuronal Na^+ responses by local application of the excitatory neurotransmitter glutamate. Short puffs of glutamate (200 μM, 10−250 ms) delivered in the vicinity of PAMAM-PEG-CG-filled neurons (Figure 5C) produced somatic Na^+ transients

TABLE 1. Intrinsic Membrane Properties[a]

property	control (n = 10)	PAMAM-PEG-CG (n = 4)
V_m, mV	−73.7 ± 1.8	−70.5 ± 1.7
R_{in}, MΩ	270.0 ± 48.7	260.9 ± 51.2
AP		
amplitude, mV	74.1 ± 2.4	71.9 ± 2.9
HW, ms	2.4 ± 0.2	2.4 ± 0.1
threshold, mV	−39.8 ± 0.8	−40.8 ± 1.1
AHP		
amplitude, mV	12.0 ± 1.4	10.2 ± 1.8
HW, ms	136.7 ± 7.4	139.1 ± 33.9
F—I slope, Hz/nA	97.0 ± 20.1	95.7 ± 10.3

[a] Values are means ± SEM. R_{in}, input resistance; V_m, resting membrane potential; AP, action potential; AHP, after hyperpolarization; HW, width at half-maximum; F—I, frequency—intensity curve. Significance: comparison between columns with two-tailed unpaired t-tests did not find any significant difference.

(Figure 5A). The amplitude of Na^+ transients increased monotonically with the number of puffs applied (R^2 = 0.993, n = 4 cells, Figure 5B). Glutamate responses were abolished by ionotropic glutamate AMPA receptor antagonist CNQX, confirming that they are due to Na^+ entry through Na^+-permeable AMPA receptors. These results demonstrate that our nanoprobe enables quantitative Na^+ measurements in live tissue preparations. Neuronal electrical activity always proved difficult to measure with Na^+ dyes, often requiring averaging multiple trials to reveal responses.[52] To investigate the efficiency of our nanoprobe, we checked whether we could detect fast Na^+ changes associated with the generation of action potentials. We stimulated afferent nerve fibers with a bipolar electrode placed in neocortical layer 4, 200 μm below the neuron filled with the sensor (Figure 5F). This stimulation procedure was shown to induce consistent neuronal electrical responses. Repeated brief electrical pulses induced detectable single-trial somatic Na^+ transients (Figure 5D). As expected, their size was much smaller than during pharmacological activation of AMPA receptors; nonetheless, it increased with the amount of stimulation (Figure 5E). There was a positive correlation between the number of stimuli and time integrated responses (R^2 = 0.761, n = 9 trials, Figure 5E). Electrically induced Na^+ responses are usually larger in small cellular compartments than in the soma, due to the slower diffusion of Na^+.[52] We measured evoked Na^+ transients in basolateral dendrites. The amplitude of responses was found to be 1 order of magnitude larger in dendrites than in the soma (Figure 5G). Na^+ channel blocker tetrodotoxin (TTX) inhibited evoked dendritic Na^+ responses (Figure 5G), showing that fluorescent transients are due to action potential firing.

Live cell responses were additionally tested in cell cultures to complement the data obtained in brain slices. HEK-293 cells permanently transfected with Na^+-coupled glutamate transporter GLT-1[59] were used as a simpler model to study the performance of the

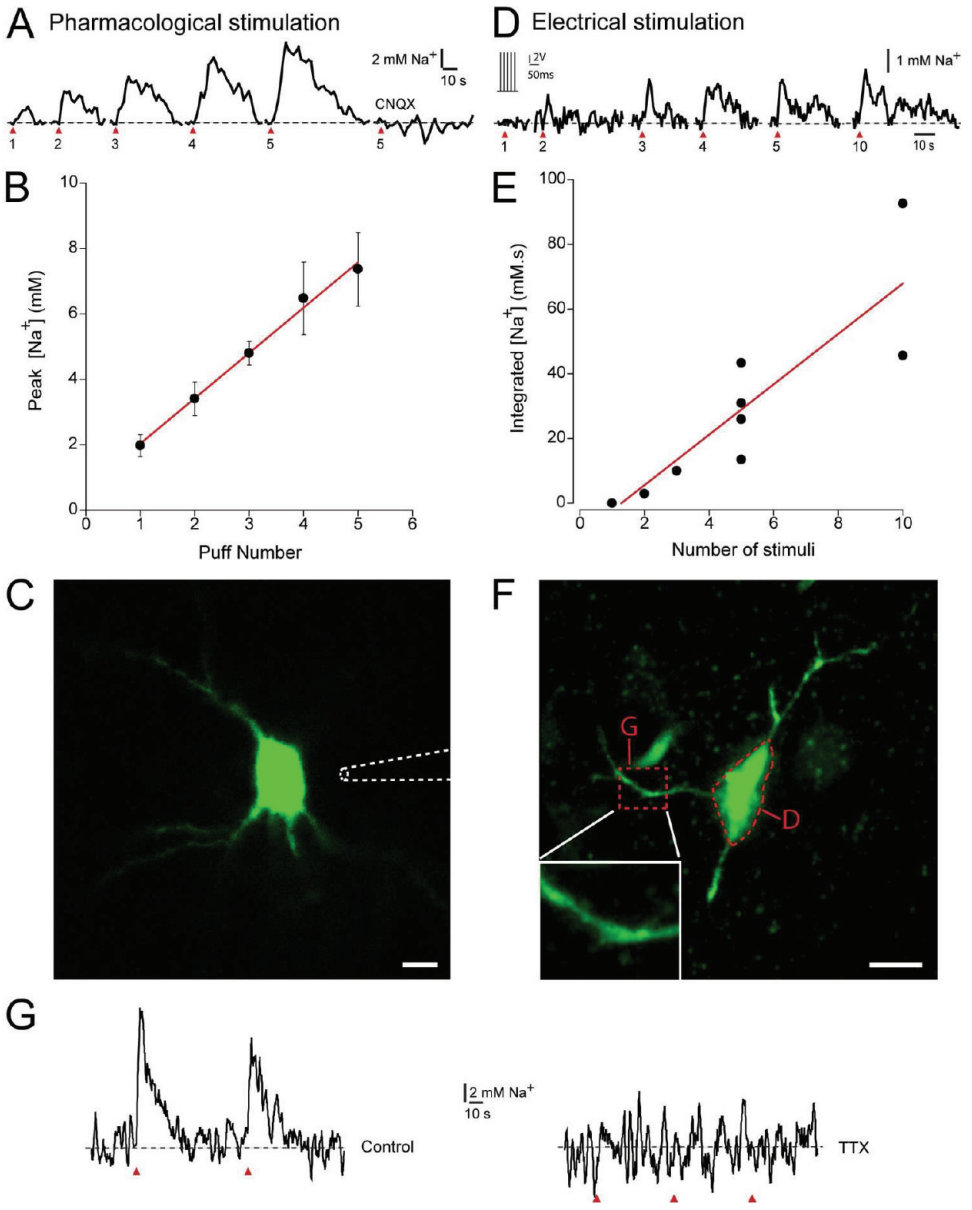

Figure 5. Time-lapse measurements of sodium responses in neurons loaded with PAMAM-PEG-CG. (A) Typical fluorescence traces measured in neuronal cell body during short local application of neurotransmitter glutamate (200 μM, 10−250 ms puffs repeated 1−5 times at 1 s interval, 60−90 s between each puff sequence) and inhibition of responses by the AMPA receptor blocker CNQX (20 μM) show that the nanoprobe reliably reports physiologically relevant [Na^+] changes *in situ*. Red arrowheads below traces indicate number of glutamate puffs in each sequence. (B) Average amplitude of [Na^+] changes plotted against the number of glutamate stimulation puffs indicate that Na^+ transients measured with the nanoprobe are proportional to stimulus intensity. Data are averages ± SEM (n = 3 cells). Red line is the linear fit to the data (R^2 = 0.993). (C) Representative fluorescence image of a cortical pyramidal neuron filled with the nanoprobe. The puff pipet is represented next to the cell soma (white dotted line). (D) Nonaveraged single-trial fluorescence transients measured in neuronal cell body during electrical stimulation of afferent nerve fibers (3−20 V, 100 μs, 50 Hz, duration 100 ms, repetition rate 1 Hz, 60−90 s between each pulse train sequence) demonstrate that the nanoprobe is suitable for detection of fast Na^+ spikes that accompany neuronal activity. Red arrowheads below traces indicate the number of pulse trains in stimulus. (E) Time integral values of individual [Na^+] transients plotted against corresponding number of pulse trains in the stimulus evidence a monotonic relationship between stimulus and probe's response. This graph suggests that the nanoprobe can give quantitative estimates of neuronal activity. Red line is the linear fit to the data (R^2 = 0.761, n = 3 cells). (F) Representative fluorescence image of a cortical pyramidal neuron showing regions where somatic and dendritic recordings were done (red dotted lines; letters refer to traces in the current figure). Inset shows a magnification of the dendritic region. (G) Fluorescent signals measured in dendrites during electrical stimulation (left) prove that the nanoprobe is usable for detection of Na^+-dependent events, such postsynaptic activity, that occur in small neuronal compartments. These transients were inhibited by their by Na^+ channel blocker TTX (1 μM, right). Scale bars, 10 μm.

nanoprobe *in situ* (Figure 6A). Glutamate (200 μM, 2 min) induced a reversible increase PAMAM-PEG-CG fluorescence due to the influx of Na^+ accompanying the uptake of glutamate by these cells (Figure 6C).

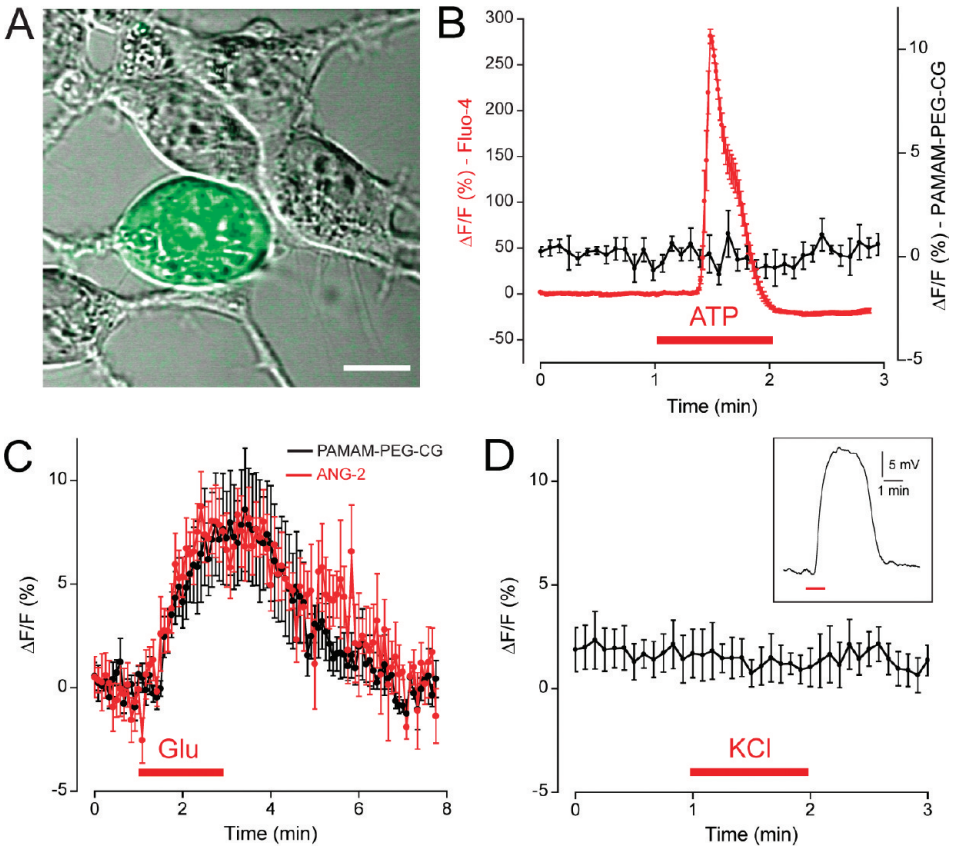

Figure 6. Sodium responses measured with PAMAM-PEG-CG in HEK-293 cells expressing glutamate transporter GLT-1. (A) Fluorescence image of a HEK-293 cell filled with PAMAM-PEG-CG by single-cell electroporation superimposed to a DIC image of the cell culture. (B) ATP (100 μM) superfusion induced large Ca^{2+} transients in HEK-293 cells loaded with Ca^{2+}-sensitive dye Fluo-4 AM (red trace). No Ca^{2+}-dependent transients were detected in cells filled with PAMAM-PEG-CG (black trace), demonstrating that Na^+ events observed during neuronal activity with the nanoprobe were not affected by the simultaneously occurring changes in $[Ca^{2+}]$. (C) Glutamate (200 μM) application on HEK-293 cells induced large Na^+ increases that were detected by both PAMAM-PEG-CG (black trace) and new Na^+ dye ANG-2 AM (red trace). Our nanoprobe thus achieves similar performance *in situ* than the new generation of Na^+ dyes (D) Superfusion of KCl (25 mM) resulted in depolarization HEK-293 cells as shown by current-clamp recording (membrane potential trace in inset) but did not alter nanoprobe fluorescence, ruling out a voltage-dependent dye-trapping artifact. Scale bar, 10 μm.

We performed the same measurements with Asante Natrium Green-2 (ANG-2), a recently reported sodium dye (Figure 6C). ANG-2 response to glutamate was identical to the response of the nanoprobe (peak amplitude: 7.78 ± 1.55 *vs* 7.78 ± 2.62% $\Delta F/F_o$, respectively, $p = 0.998$). To verify that the events we observed in neurons were not due to detection of Ca^{2+} transients, we measured nanoprobe fluorescence during Ca^{2+} changes in HEK-293 cells. Application of ATP (100 μM, 1 min), despite producing a large increase in cytosolic $[Ca^{2+}]$, did not lead to any detectable signal with PAMAM-PEG-CG (Figure 6B), confirming the absence of Ca^{2+} dependence demonstrated *in vitro*. PEG coating of the nanoparticle could be another source of artifacts. By favoring the partitioning of the probe in the plasma membrane, it could induce voltage-dependent dye-trapping and corresponding fluorescence changes. KCl (25 mM, 1 min) induced a large depolarization of cells (24 ± 2 mV, Figure 6D inset) but no change in probe's fluorescence (Figure 6D), ruling out any interference of membrane potential changes in our Na^+ measurements in neurons.

Collectively, these data indicate that PAMAM-PEG-CG is an efficient Na^+ nanosensor that can be used for the real-time detection of cytosolic Na^+ transients in live tissue during physiological activity. Sensitivity of the nanoprobe was 3.3% fluorescence change/mM (%$\Delta F/F$/mM), similar to free CG (3.2%$\Delta F/F$/mM) and to existing PEBBLE Na^+ nanosensor (2.7%$\Delta F/F$/mM[27]), but lower than quantum-dot-based nanosensor (12.5%$\Delta F/F$/mM[27]). *In situ* sensitivity was smaller than the one measured *in vitro* (1.3%$\Delta F/F$/mM) as expected from a higher viscosity and interaction with proteins in the cytosol. The linear dependence of the probe's response for $[Na^+]$ values observed during physiological activity indicates that PAMAM-PEG-CG can be used for quantitative $[Na^+]$ measurements.[52] A matter of concern is whether the probe truly reflects the bulk intracellular $[Na^+]$ or only the local $[Na^+]$ in the dendrimer internal environment. It has been shown that G5 dendrimer cavities are filled with the solvent and

ions and that there is a dynamic exchange with the bulk solution.[60] Nonetheless, the positively charged interior of the dendrimer could repel Na^+ and lead to a distortion in [Na^+] readout similarly to the effect produced by surface charges.[48] However, the calibration curve we generated and the successful quantitative measurements of fast intracellular Na^+ changes demonstrate that this is not the case. The likely reason is that the positive charge density in the cavity is much lower at pH 7.4 than the charge density shown to create an unfavorable local nanoenvironment at the surface. Altogether, PAMAM-PEG-CG appears as valuable complement to existing Na^+ dyes. It supersedes historical dye SBFI for imaging in thick samples thanks to its excitation spectrum in the visible range. Its characteristics are similar to new Na^+ dye ANG.[61] Like ANG, the nanoprobe is excitable with visible light, efficiently loads cells, and reliably measures fast cellular Na^+ events. An advantage of ANG over our nanoprobe is the existence of a cell-permeant version that permits bulk loading. The nanoprobe on the other hand is more appropriate for extended time-lapse imaging thanks to a high intracellular retention time. In addition, excitation and emission spectra of both probes are different. Our nanosensor is comparable to usual green-emitting dyes, which makes it easy to use with standard imaging equipment and when dual imaging with a red-emitting reporter is needed. In contrast, ANG, which is shifted to higher wavelength, requires specific filter sets and is more likely to overlap with other frequently used costains.

CONCLUSION

In conclusion, we present a novel strategy to produce ion-sensitive nanosensors based on the use of dendrimers. We show that with this approach it is possible to improve the retention of fluorescent dyes in cells. These sensors display a high ion responsiveness and biocompatibility and enable prolonged imaging of intracellular ion dynamics. Following this design, we established a new Na^+-sensing probe and demonstrated its efficiency for imaging neuronal activity in whole brain tissue. The same principle could be applied to other existing fluorescent dyes and help generate new applications for live fluorescent imaging. Since dendrimer-based nanoprobes are straightforward to assemble, they could become an attractive tool for biologists.

METHODS

Nanoprobe Synthesis. CoroNa Green, Corona Red (Invitrogen, Carlsbad, CA, USA), and PAMAM dendrimers (Dendritic Nanotechnologies Inc., Mount Pleasant, MI, USA) stock solutions were made in methanol (MeOH). G5 PAMAM dendrimers with 1,4-diaminobutane core and either amidoamine (29 kDa, 1 equiv) or poly(ethyleneglycol) methyl ether surface (104 kDa, 1 equiv) were stirred with 1.2 equiv of CG (0.48 mM) at room temperature for 30 min. To probe the role of electrostatic interactions in the complexation of the dye, a batch of PAMAM-PEG-CG was prepared at pH 6.0. G4.5 PAMAM dendrimer with 1,4-diaminobutane core and sodium carboxylic surface (0.24 μmol, 10 wt %, 1 equiv) was stirred with 1.2 equiv of CR at room temperature for 30 min. An equal volume of HEPES buffer (10 mM, pH 7.4, HB) was added. The pH was adjusted if necessary by addition of HCl. The mixture was stirred uncovered overnight to allow slow evaporation of MeOH. Remaining MeOH was evaporated under reduced pressure for 2.5 h at 30 °C. The preparation was resuspended in HB and ultrafiltered with a 3 kDa cutoff membrane (Millipore, Billerica, MA, USA). This procedure was repeated four times to ensure that all unbound dye was removed. The flow-through was collected for quantification of the fraction of the dye associated with the dendrimer. Dendrimer–dye complexes retained on the ultrafiltration membrane were resuspended in HB at a concentration equivalent to 1 mM of the dye. They were filtered with a 0.22 μm filter to remove aggregates and stored at −20 °C until used. All manipulations and storage were done in the dark to avoid photobleaching of the dye. Under these conditions, nanoprobes remained stable for many months.

UV–Vis Spectrometry. UV–vis absorbance spectra of fluorescent probes and optical density measurements were measured on a Nanodrop 1000 spectrophotometer (Thermo Fisher Scientific Inc., Waltham, MA, USA) in 1 μL volume. Quantifications of unbound dye concentration in ultrafiltration flow-through were done using the Beer–Lambert law with molar extinction coefficients of 68 000 M^{-1} cm^{-1} for CG and 92 000 M^{-1} cm^{-1} for CR.

Acid–Base Titration. Determination of the pK_a of CG pK_a was done by a spectrophotometric method, taking advantage of the different absorbance of protonated and deprotonated forms of CG. Solutions of different pH values based on a citrate buffer (pH 2–6) or on a HEPES buffer (pH 6.5–8.5) were mixed with 200 μM CG. Absorbance of CG in each solution was done on a Cary 50 Bio UV–vis spectrophotometer (Agilent Technologies, Santa Clara, CA, USA). The apparent pK_a value was obtained from a Boltzmann-type equation fit of the absorbance *versus* pH plot.

Spectrofluorimetry and Fluorescence Anisotropy. Fluorescence emission spectra and steady-state anisotropy measurements were done on a Cary Eclipse fluorescence spectrophotometer (Agilent Technologies, Santa Clara, CA, USA) using 10 μM of fluorescent probes in HB at pH 7.4 with 20 mM Na^+. Fluorescence spectra were blank subtracted and represented as the intensity normalized to the peak value. Anisotropy was calculated according to the following equation:

$$r = \frac{I_{vv} - GI_{vh}}{I_{vv} + 2GI_{vh}}$$

where I_{vv} and I_{vh} are the intensities of fluorescence emission components parallel and perpendicular to the excitation light polarization, respectively, and G a correction factor defined by $G = I_{hv}/I_{hh}$.

Nanoprobe Calibration. *In vitro* calibrations for Na^+, K^+, Ca^{2+}, and pH were done by mixing calibration solutions having known [Na^+], [K^+], [Ca^{2+}], and pH values with 10 μM of fluorescent probes. Fluorescence emission spectra were obtained with a Cary Eclipse fluorescence spectrophotometer. Fluorescence intensities of the emission maxima were plotted against known electrolyte concentrations to generate calibration curves. Na^+ calibration was performed with intracellular-like solutions containing (mM) 165 Na^+ + K^+, 30 Cl^-, 135 gluconate, 10 HEPES, pH 7.4. K^+ calibration solutions contained (mM) 0–200 K^+, 20 Na^+, 10 HEPES, pH 7.4. Calibration solutions for pH contained (mM) 145 K^+, 20 Na^+, 30 Cl^-, 135 gluconate 10 HEPES, pH 6.5–8.0. Sensitivity to Ca^{2+} was tested using

solutions of defined free [Ca^{2+}] in the presence of 1 mM EGTA as calculated using the Maxchelator software (Chris Patton, Stanford University, http://www.stanford.edu/~cpatton/maxc.html). They contained 138 K^+, 8 Na^+, 18–20 Cl^-, 138 gluconate, 10 HEPES, 5 Mg^{2+}, 1 EGTA, 0–1 Ca^{2+}, pH 7.4.

In situ calibration was performed as previously described.[62] Briefly, cell membrane was permeabilized for monovalent cations using 6 μg/mL gramicidin and 10 μM monensin with simultaneous inhibition the Na^+/K^+-ATPase using 1 mM ouabain. Cells were then sequentially perfused with the same Na^+ calibration solutions as described above, with [Na^+] varying from 0 to 50 mM.

Electron Microscopy. PAMAM-PEG-CG nanoparticles were diluted at 1:1000 in water. Formvar carbon-coated EM grids were incubated for 5 min floating on a drop of diluted nanoparticles. After a short wash with water, they were stained for 2 min with 4% (w/v) uranyl acetate in water. The grids were air-dried. Images were taken with a transmission electron microscope (CM100, Philips Electron Optics, now FEI Company, Eindhoven, The Netherlands) operated at 80 keV with a MegaView III camera (Olympus Soft Imaging Solutions GmbH, Münster, Germany). Particle measurements were done with Image J (Rasband, W.S., ImageJ, U.S. National Institutes of Health, Bethesda, MA, USA, http://imagej.nih.gov/ij/, 1997–2011). Eight bits grayscale images were background subtracted with a rolling-ball algorithm, median filtered, and automatically thresholded with the maximum entropy method. Particles were automatically analyzed in the resulting binary image after application of a watershed algorithm to separate contiguous particles, using an area criterion of 100–700 px^2. Particles were modeled as ellipses, and the particle radius was calculated as the average of minor and major radii.

Brain Slice Preparation. All experimental procedures were carried out according to the Swiss Ordinance on Animal Experimentation. Sprague–Dawley rats (P14-P23) were decapitated, and 300 μm thick transverse slices of somatosensory cortex were cut in cold extracellular solution using a vibrating microslicer (VT1000, Leica Microsystems, Heerbrugg). Slices were incubated at 34 °C for 1 h and then held at room temperature (20–22 °C) in extracellular solution until recording.

Cell Cultures. HEK-293 stably expressing glutamate transporter GLT-1 were kindly provided by Dr. Marcus Rattray (University of Reading, UK).[59] Cells were grown in Dulbecco's modified Eagle's medium containing 2 mM L-glutamine, 4500 mg/L D-glucose, and 110 mg/L sodium pyruvate, supplemented with 10% heat-inactivated fetal bovine serum (FBS), 400 μg/mL G-418 (Geneticin), and maintained in 95% O_2/5% CO_2 at 37 °C. They were plated 48 h before experiments on uncoated glass coverslips and used at 50–70% confluence.

Single-Cell Electroporation. The nanoprobe (1 mM) was added to a pipet solution containing (mM) 130 K-gluconate, 5 NaCl, 10 HEPES (adjusted to pH 7.3 with KOH), and loaded in a 4–5 MΩ glass pipet. The pipet was lowered in the slice and approached to the target neuron until close contact was obtained between the membrane and the tip of the pipet. A short (1–10 ms) voltage pulse (10–15 V) was applied to the pipet solution in order to simultaneously expel the fluorescent probe from the pipet and electroporate the cell membrane. Cell loading was monitored with a laser scanning confocal microscope (see below). Pipette could be moved to different cells in sequence to obtain multicell loading. The same procedure was adapted to fill HEK-293 cells.

Fluorescence Imaging. Fluorescence acquisitions were done on a LSM 510 Meta laser scanning confocal microscope with a 40×, 0.8 NA water-dipping objective (Carl Zeiss, Jena) using either a 488 nm argon laser (CG-based probes, ANG-2, Fluo-4) or a 543 nm helium–neon laser (CR-based probes) for excitation. Fluorescence emission was collected either with a photomultiplier tube or on a spectral detector (Meta detector). To assess the diffusion of the probes in recorded neurons, z-stacks were acquired at 1 μm intervals. Three-dimensional reconstructions of these neurons were performed from z-stacks using the Imaris software package (Bitplane, Zurich, Switzerland) and represented in 2D as maximum intensity projections. To monitor the fluorescent baseline stability and measure cells' responses to stimulations, acquisitions of image time series were done in frame mode (512 × 512 pixels) at a rate of 1–2 Hz. Fluorescence intensity over time traces were drawn from regions of interest with Image J (Rasband, W.S., http://imagej.nih.gov/ij/), corrected for background and represented as fractional fluorescence changes over the baseline ($\Delta F/F$) with Igor Pro (Wavemetrics Inc., Portland, OR, USA).

Electrophysiology. Brain slices were continuously superfused at a rate of 2 mL/min with an extracellular solution containing (mM) 125 NaCl, 2.5 KCl, 26 $NaHCO_3$, 1.25 NaH_2PO_4, 2 $CaCl_2$ and 1 $MgCl_2$, 10 glucose, bubbled with 95% O_2 and 5% CO_2. Borosilicate glass pipettes with resistances of 4.0–5.0 MΩ containing (mM) 130 K-gluconate, 5 NaCl, 10 HEPES, 10 phosphocreatine, 2 Mg-ATP, 0.5 Na_2-GTP (adjusted to pH 7.3 with KOH) were used to obtain whole-cell recordings. PAMAM-PEG-CG 10 μM was added to the pipet solution where indicated. Signals were amplified using a Multiclamp 700B amplifier (Molecular Devices, Sunnyvale, CA, USA), filtered at 3 kHz, digitized at 10 kHz using Digidata 1440 (Molecular Devices), and acquired with pClamp 10 electrophysiology package (Molecular Devices). In voltage clamp mode, cells were held at −70 mV. For current clamp recording, cells were kept with 0 holding current injected. Access resistance and holding current were monitored throughout the experiments, and data were discarded when these parameters increased over 30 MΩ or below −30 pA, respectively. Intrinsic membrane properties were recorded after a settling time of ≥10 min. Electrophysiology recordings were analyzed with the pClamp 10 (Molecular Probes). Current clamp recording were also performed on HEK-293 cells to measure the amount of depolarization induced by superfusion of 25 mM KCl.

Neuronal Stimulations. Pharmacological stimulations were done by local application with a glass pipet of tip diameter 1–2 μm, filled with glutamate (200 μM in extracellular solution). The pipet was placed at 10 μm from the soma, and pressure pulses of 10–250 ms, 1–2 psi were applied to the back of the pipet with a Pressure System II (The Toohey Company, Fairfield, NJ, USA) to expel the drug. Electrical stimulations were performed using tungsten parallel bipolar electrodes (WPI, Sarasota, FL, USA) placed in cortical layer 4, below the layer 2/3 target neuron. Depolarizing voltage pulse trains (3–20 V, 100 μs, 50 Hz, duration 100 ms, repetition rate 1 Hz) were generated with an isolated constant voltage stimulator (DS2A, Digitimer, Letchworth, UK). Time interval between two consecutive pharmacological or electrical stimuli was 60 to 90 s.

Measurements in Cell Cultures. The nanoprobe was introduced in HEK-293 cells by single-cell electroporation as described earlier. Cell-permeant dyes were loaded by incubating HEK-293 cultures in a solution containing (mM) 135 NaCl, 5.4 KCl, 20 HEPES, 1.3 $CaCl_2$, 0.8 $MgSO_4$, 0.78 NaH_2PO_4, 20 glucose (pH 7.4), supplemented with 0.1% Pluronic F-127 (Invitrogen, Carlsbad, CA), in the presence of 12 μM ANG-2 AM or 6 μM Fluo-4 AM for 40 min at 37 °C. For imaging, cultures were superfused with to a solution containing (mM) 160 NaCl, 5.4 KCl, 20 HEPES, 1.3 $CaCl_2$, 0.8 $MgSO_4$, 0.78 NaH_2PO_4, 5 glucose (pH 7.4), bubbled with air and maintained at 37 °C. Drugs and KCl solution were added to the superfusion.

Data Processing. Numerical data were collected in Excel (Microsoft, Redmond, WA, USA) or Open office (http://www.openoffice.org/) spreadsheets. Plots and curve fittings and statistical analysis were done with Kaleidagraph (Synergy Software, Reading, PA, USA) and Origin (OriginLab, Northampton, MA, USA). Representative images were assembled with Image J (Rasband, W.S., http://imagej.nih.gov/ij/). Pairwise comparisons were done where relevant with two-tailed *t*-tests. Data are given as average ± SEM.

Drugs. Glutamate, AMPA, and ATP were obtained from Sigma-Aldrich (St Louis, MO, USA), and TTX and CNQX were from Biotrend (Anawa Trading, Switzerland). They were prepared as stock solutions in water, except CNQX that was prepared in DMSO. Final dilution in experimental solutions was 1/1000.

Conflict of Interest: The authors declare no competing financial interest.

Acknowledgment. This study was supported by Grant Nos. 310A0-119827 and 31003A-135720 of the Swiss National Science Foundation to J.-Y.C. We thank Dr. Bruno Humbel, Electron Microscopy Facility, University of Lausanne, for his help on performing EM images of the nanoprobe, Prof. Dirk Fasshauer, University of Lausanne, for his help with fluorescence spectrometry, and Dr. Marcus Rattray, Reading School of Pharmacy, University of Reading, United Kingdom, for kindly providing a clone of HEK-293 cells stably expressing GLT-1.

Supporting Information Available: Free CG and PAMAM-PEG-CG absorbance spectra. This material is available free of charge *via* the Internet at http://pubs.acs.org.

REFERENCES AND NOTES

1. Lichtman, J. W.; Conchello, J. A. Fluorescence Microscopy. *Nat. Methods* **2005**, *2*, 910–919.
2. Yuste, R. Fluorescence Microscopy Today. *Nat. Methods* **2005**, *2*, 902–904.
3. Taraska, J. W.; Zagotta, W. N. Fluorescence Applications in Molecular Neurobiology. *Neuron* **2010**, *66*, 170–189.
4. Helmchen, F.; Denk, W. Deep Tissue Two-Photon Microscopy. *Nat. Methods* **2005**, *2*, 932–940.
5. Grewe, B. F.; Helmchen, F. Optical Probing of Neuronal Ensemble Activity. *Curr. Opin. Neurobiol.* **2009**, *19*, 520–529.
6. Cannell, M. B.; Cody, S. H. Fluorescent Ion Measurement. In *Handbook of Biological Confocal Microscopy*, 3rd ed.; Pawley, J. B., Ed.; SpringerScience+Business Media: New York, 2006; pp 736−745.
7. Minta, A.; Tsien, R. Y. Fluorescent Indicators for Cytosolic Sodium. *J. Biol. Chem.* **1989**, *264*, 19449–19457.
8. Meier, S. D.; Kovalchuk, Y.; Rose, C. R. Properties of the New Fluorescent Na^+ Indicator Corona Green: Comparison with Sbfi and Confocal Na^+ Imaging. *J. Neurosci. Methods* **2006**, *155*, 251–259.
9. Jezek, P.; Mahdi, F.; Garlid, K. D. Reconstitution of the Beef Heart and Rat Liver Mitochondrial K^+/H^+ (Na^+/H^+) Antiporter. Quantitation of K^+ Transport with the Novel Fluorescent Probe, Pbfi. *J. Biol. Chem.* **1990**, *265*, 10522–10526.
10. Verkman, A. S.; Sellers, M. C.; Chao, A. C.; Leung, T.; Ketcham, R. Synthesis and Characterization of Improved Chloride-Sensitive Fluorescent Indicators for Biological Applications. *Anal. Biochem.* **1989**, *178*, 355–361.
11. Neher, E.; Augustine, G. J. Calcium Gradients and Buffers in Bovine Chromaffin Cells. *J. Physiol.* **1992**, *450*, 273–301.
12. Despa, S.; Vecer, J.; Steels, P.; Ameloot, M. Fluorescence Lifetime Microscopy of the Na^+ Indicator Sodium Green in HeLa Cells. *Anal. Biochem.* **2000**, *281*, 159–175.
13. Kang, J.; Arcuino, G.; Nedergaard, M. Calcium Imaging of Identified Astrocytes in Hippocampal Slices. In *Imaging in Neuroscience and Development: A Laboratory Manual*; Yuste, R., Konnerth, A., Eds; Cold Spring Harbor Laboratory Press: Plainview, NY, 2005; pp 290−297.
14. Szmacinski, H.; Lakowicz, J. R. Sodium Green as a Potential Probe for Intracellular Sodium Imaging Based on Fluorescence Lifetime. *Anal. Biochem.* **1997**, *250*, 131–138.
15. Dubach, J. M.; Das, S.; Rosenzweig, A.; Clark, H. A. Visualizing Sodium Dynamics in Isolated Cardiomyocytes Using Fluorescent Nanosensors. *Proc. Natl. Acad. Sci. U.S.A.* **2009**, *106*, 16145–16150.
16. Han, M.; Gao, X.; Su, J. Z.; Nie, S. Quantum-Dot-Tagged Microbeads for Multiplexed Optical Coding of Biomolecules. *Nat. Biotechnol.* **2001**, *19*, 631–635.
17. Park, J. H.; Gu, L.; von Maltzahn, G.; Ruoslahti, E.; Bhatia, S. N.; Sailor, M. J. Biodegradable Luminescent Porous Silicon Nanoparticles for *In Vivo* Applications. *Nat. Mater.* **2009**, *8*, 331–336.
18. Anilkumar, P.; Wang, X.; Cao, L.; Sahu, S.; Liu, J. H.; Wang, P.; Korch, K.; Tackett, K. N., II; Parenzan, A.; Sun, Y. P. Toward Quantitatively Fluorescent Carbon-Based "Quantum" Dots. *Nanoscale* **2011**, *3*, 2023–2027.
19. Mohan, N.; Chen, C. S.; Hsieh, H. H.; Wu, Y. C.; Chang, H. C. *In Vivo* Imaging and Toxicity Assessments of Fluorescent Nanodiamonds in *Caenorhabditis elegans*. *Nano Lett.* **2010**, *10*, 3692–3699.
20. Welsher, K.; Liu, Z.; Daranciang, D.; Dai, H. Selective Probing and Imaging of Cells with Single Walled Carbon Nanotubes as Near-Infrared Fluorescent Molecules. *Nano Lett.* **2008**, *8*, 586–590.
21. Dhanaraj, J.; Jagannathan, R.; Kutty, T. R. N.; Lu, C. H. Photoluminescence Characteristics of Y2O3:$Eu3^+$ Nanophosphors Prepared Using Sol−Gel Thermolysis. *J. Phys. Chem. B* **2001**, *105*, 11098–11105.
22. Tong, L.; Cobley, C. M.; Chen, J.; Xia, Y.; Cheng, J. X. Bright Three-Photon Luminescence from Gold/Silver Alloyed Nanostructures for Bioimaging with Negligible Photothermal Toxicity. *Angew. Chem., Int. Ed.* **2010**, *49*, 3485–3488.
23. Ruedas-Rama, M. J.; Wang, X.; Hall, E. A. A Multi-Ion Particle Sensor. *Chem. Commun.* **2007**, 1544–1546.
24. Ruedas-Rama, M. J.; Orte, A.; Hall, E. A.; Alvarez-Pez, J. M.; Talavera, E. M. Quantum Dot Photoluminescence Lifetime-Based pH Nanosensor. *Chem. Commun.* **2011**, *47*, 2898–2900.
25. Snee, P. T.; Somers, R. C.; Nair, G.; Zimmer, J. P.; Bawendi, M. G.; Nocera, D. G. A Ratiometric CdSe/ZnS Nanocrystal Ph Sensor. *J. Am. Chem. Soc.* **2006**, *128*, 13320–13321.
26. Tomasulo, M.; Yildiz, I.; Kaanumalle, S. L.; Raymo, F. M. pH-Sensitive Ligand for Luminescent Quantum Dots. *Langmuir* **2006**, *22*, 10284–10290.
27. Dubach, J. M.; Harjes, D. I.; Clark, H. A. Ion-Selective Nanooptodes Incorporating Quantum Dots. *J. Am. Chem. Soc.* **2007**, *129*, 8418–8419.
28. Dubach, J. M.; Harjes, D. I.; Clark, H. A. Fluorescent Ion-Selective Nanosensors for Intracellular Analysis with Improved Lifetime and Size. *Nano Lett.* **2007**, *7*, 1827–1831.
29. Brasuel, M.; Kopelman, R.; Kasman, I.; Miller, T. J.; Philbert, M. A. Ion Concentrations in Live Cells from Highly Selective Ion Correlation Fluorescent Nano-Sensors for Sodium Sensors. *Proc. IEEE* **2002**, *1*, 288–292.
30. Buck, S. M.; Xu, H.; Brasuel, M.; Philbert, M. A.; Kopelman, R. Nanoscale Probes Encapsulated by Biologically Localized Embedding (Pebbles) for Ion Sensing and Imaging in Live Cells. *Talanta* **2004**, *63*, 41–59.
31. Johnson, I. D. Practical Considerations in the Selection and Application of Fluorescent Probes. In *Handbook of Biological Confocal Microscopy*, 3rd ed.; Pawley, J. B., Ed.; SpringerScience+Business Media: New York, 2006; pp 353−367.
32. Kreitzer, A. C.; Gee, K. R.; Archer, E. A.; Regehr, W. G. Monitoring Presynaptic Calcium Dynamics in Projection Fibers by *In Vivo* Loading of a Novel Calcium Indicator. *Neuron* **2000**, *27*, 25–32.
33. Grayson, S. M.; Frechet, J. M. Convergent Dendrons and Dendrimers: From Synthesis to Applications. *Chem. Rev.* **2001**, *101*, 3819–3868.
34. Svenson, S.; Tomalia, D. A. Dendrimers in Biomedical Applications--Reflections on the Field. *Adv. Drug Delivery Rev.* **2005**, *57*, 2106–2129.
35. Menjoge, A. R.; Kannan, R. M.; Tomalia, D. A. Dendrimer-Based Drug and Imaging Conjugates: Design Considerations for Nanomedical Applications. *Drug Discovery Today* **2010**, *15*, 171–185.
36. Jansen, J. F.; de Brabander-van den Berg, E. M.; Meijer, E. W. Encapsulation of Guest Molecules into a Dendritic Box. *Science* **1994**, *266*, 1226–1229.
37. Kline, K. K.; Morgan, E. J.; Norton, L. K.; Tucker, S. A. Encapsulation and Quantification of Multiple Dye Guests in Unmodified Poly(amidoamine) Dendrimers as a Function of Generation. *Talanta* **2009**, *78*, 1489–1491.
38. Tomalia, D. A.; Frechet, J. M. Discovery of Dendrimers and Dendritic Polymers: A Brief Historical Perspective. *J. Polym. Sci., Part A: Polym. Chem.* **2002**, *40*, 2719–2728.
39. Wangler, C.; Moldenhauer, G.; Saffrich, R.; Knapp, E. M.; Beijer, B.; Schnolzer, M.; Wangler, B.; Eisenhut, M.; Haberkorn, U.; Mier, W. PAMAM Structure-Based Multifunctional Fluorescent Conjugates for Improved Fluorescent Labelling of Biomacromolecules. *Chemistry* **2008**, *14*, 8116–8130.

40. Jansen, J. F.; Meijer, E. W. Bengal Rose@Dendritic Box. *Macromol. Symp.* **1996**, *102*, 27–33.
41. Baars, M. W.; Kleppinger, R.; Koch, M. H.; Yeu, S. L.; Meijer, E. W. The Localization of Guests in Water-Soluble Oligoethyleneoxy-Modified Poly(propylene imine) Dendrimers. *Angew. Chem., Int. Ed.* **2000**, *39*, 1285–1288.
42. Baars, M. W.; Meijer, E. W. Host–Guest Chemistry of Dendritic Molecules. In *Topics in Current Chemistry: Dendrimers II*; Vögtle, F., Ed.; Springer: Berlin/Heidelberg, 2000; Vol. 210, pp 131–182.
43. Leisner, D.; Imae, T. Polyelectrolyte Behavior of an Interpolyelectrolyte Complex Formed in Aqueous Solution of a Charged Dendrimer and Sodium Poly(L-glutamate). *J. Phys. Chem. B* **2003**, *107*, 13158–13167.
44. El-Sayed, M.; Kiani, M. F.; Naimark, M. D.; Hikal, A. H.; Ghandehari, H. Extravasation of Poly(amidoamine) (PAMAM) Dendrimers across Microvascular Network Endothelium. *Pharm. Res.* **2001**, *18*, 23–28.
45. Domanski, D. M.; Klajnert, B.; Bryszewska, M. Incorporation of Fluorescent Probes into Pamam Dendrimers. *Bioelectrochemistry* **2004**, *63*, 193–197.
46. Arun, K. T.; Jayaram, D. T.; Avirah, R. R.; Ramaiah, D. β-Cyclodextrin as a Photosensitizer Carrier: Effect on Photophysical Properties and Chemical Reactivity of Squaraine Dyes. *J. Phys. Chem. B* **2011**, *115*, 7122–7128.
47. Imhof, A.; Megens, M.; Engelberts, J. J.; de Lang, D. T. N.; Sprik, R.; Vos, W. L. Spectroscopy of Fluorescein (FITC) Dyed Colloidal Silica Spheres. *J. Phys. Chem. B* **1999**, *103*, 1408–1415.
48. Riedinger, A.; Zhang, F.; Dommershausen, F.; Rocker, C.; Brandholt, S.; Nienhaus, G. U.; Koert, U.; Parak, W. J. Ratiometric Optical Sensing of Chloride Ions with Organic Fluorophore–Gold Nanoparticle Hybrids: A Systematic Study of Design Parameters and Surface Charge Effects. *Small* **2010**, *6*, 2590–2597.
49. Balzani, V.; Ceroni, P.; Gestermann, S.; Gorka, M.; Kauffmann, C.; Vogtle, F. Fluorescent Guests Hosted in Fluorescent Dendrimers. *Tetrahedron* **2002**, *58*, 629–637.
50. Zhang, F.; Ali, Z.; Amin, F.; Feltz, A.; Oheim, M.; Parak, W. J. Ion and pH Sensing with Colloidal Nanoparticles: Influence of Surface Charge on Sensing and Colloidal Properties. *ChemPhysChem* **2010**, *11*, 730–735.
51. Nevian, T.; Helmchen, F. Calcium Indicator Loading of Neurons Using Single-Cell Electroporation. *Pflugers Arch.* **2007**, *454*, 675–688.
52. Fleidervish, I. A.; Lasser-Ross, N.; Gutnick, M. J.; Ross, W. N. Na^+ Imaging Reveals Little Difference in Action Potential-Evoked Na^+ Influx between Axon and Soma. *Nat. Neurosci.* **2010**, *13*, 852–860.
53. Fritzinger, B.; Scheler, U. Scaling Behaviour of PAMAM Dendrimers Determined by Diffusion NMR. *Macromol. Chem. Phys.* **2005**, *206*, 1288–1291.
54. Hedden, R. C.; Bauer, B. J. Structure and Dimensions of PAMAM/PEG Dendrimer-Star Polymers. *Macromolecules* **2003**, *36*, 1829–1835.
55. Prosa, T. J.; Bauer, B. J.; Amis, E. J. From Stars to Spheres: A SAXS Analysis of Dilute Dendrimer Solutions. *Macromolecules* **2001**, *34*, 4897–4906.
56. Tomalia, D. A.; Naylor, A. M.; Goddard, W. A. Starburst Dendrimers: Molecular-Level Control of Size, Shape, Surface Chemistry, Topology, and Flexibility from Atoms to Macroscopic Matter. *Angew. Chem., Int. Ed. Engl.* **1990**, *29*, 138–175.
57. Yang, H.; Lopina, S. T.; DiPersio, L. P.; Schmidt, S. P. Stealth Dendrimers for Drug Delivery: Correlation between PEGylation, Cytocompatibility, and Drug Payload. *J. Mater. Sci. Mater. Med.* **2008**, *19*, 1991–1997.
58. Kim, Y.; Klutz, A. M.; Jacobson, K. A. Systematic Investigation of Polyamidoamine Dendrimers Surface-Modified with Poly(ethylene glycol) for Drug Delivery Applications: Synthesis, Characterization, and Evaluation of Cytotoxicity. *Bioconjugate Chem.* **2008**, *19*, 1660–1672.
59. Peacey, E.; Miller, C. C.; Dunlop, J.; Rattray, M. The Four Major N- and C-Terminal Splice Variants of the Excitatory Amino Acid Transporter Glt-1 Form Cell Surface Homomeric and Heteromeric Assemblies. *Mol. Pharmacol.* **2009**, *75*, 1062–1073.
60. Maiti, P. K.; Çagn, T.; Lin, S.-T.; Goddard, W. A. Effect of Solvent and pH on the Structure of Pamam Dendrimers. *Macromolecules* **2005**, *38*, 979–991.
61. Lamy, C. M.; Chatton, J. Y. Optical Probing of Sodium Dynamics in Neurons and Astrocytes. *Neuroimage* **2011**, *58*, 572–578.
62. Chatton, J. Y.; Marquet, P.; Magistretti, P. J. A Quantitative Analysis of L-Glutamate-Regulated Na^+ Dynamics in Mouse Cortical Astrocytes: Implications for Cellular Bioenergetics. *Eur. J. Neurosci.* **2000**, *12*, 3843–3853.